

# Bestrophin 1 is indispensable for volume regulation in human retinal pigment epithelium cells

Andrea Milenkovic<sup>a</sup>, Caroline Brandl<sup>a,b</sup>, Vladimir M. Milenkovic<sup>c</sup>, Thomas Jendryke<sup>c</sup>, Lalida Sirianant<sup>d</sup>, Potchanart Wanitchakool<sup>d</sup>, Stephanie Zimmermann<sup>a</sup>, Charlotte M. Reiff<sup>e</sup>, Franziska Horling<sup>a</sup>, Heinrich Schrewe<sup>f</sup>, Rainer Schreiber<sup>d</sup>, Karl Kunzelmann<sup>d</sup>, Christian H. Wetzel<sup>c</sup>, and Bernhard H. F. Weber<sup>a,1</sup>

<sup>a</sup>Institute of Human Genetics, <sup>c</sup>Department of Psychiatry and Psychotherapy, Molecular Neurosciences, and <sup>d</sup>Department of Physiology, University of Regensburg, 93053 Regensburg, Germany; <sup>b</sup>University Eye Clinic, 93053 Regensburg, Germany; <sup>e</sup>Eye Center, Albert-Ludwigs-University of Freiburg, 79106 Freiburg, Germany; and <sup>f</sup>Department of Developmental Genetics, Max Planck Institute for Molecular Genetics, 14195 Berlin, Germany

Edited by Jeremy Nathans, Johns Hopkins University, Baltimore, MD, and approved March 16, 2015 (received for review October 1, 2014)

In response to cell swelling, volume-regulated anion channels (VRACs) participate in a process known as regulatory volume decrease (RVD). Only recently, first insight into the molecular identity of mammalian VRACs was obtained by the discovery of the leucine-rich repeats containing 8A (LRRC8A) gene. Here, we show that bestrophin 1 (BEST1) but not LRRC8A is crucial for volume regulation in human retinal pigment epithelium (RPE) cells. Whole-cell patch-clamp recordings in RPE derived from human-induced pluripotent stem cells (hiPSC) exhibit an outwardly rectifying chloride current with characteristic functional properties of VRACs. This current is severely reduced in hiPSC-RPE cells derived from macular dystrophy patients with pathologic BEST1 mutations. Disruption of the orthologous mouse gene (*Best1*<sup>-/-</sup>) does not result in obvious retinal pathology but leads to a severe subfertility phenotype in agreement with minor endogenous expression of *Best1* in murine RPE but highly abundant expression in mouse testis. Sperm from *Best1*<sup>-/-</sup> mice showed reduced motility and abnormal sperm morphology, indicating an inability in RVD. Together, our data suggest that the molecular identity of VRACs is more complex—that is, instead of a single ubiquitous channel, VRACs could be formed by cell type- or tissue-specific subunit composition. Our findings provide the basis to further examine VRAC diversity in normal and diseased cell physiology, which is key to exploring novel therapeutic approaches in VRAC-associated pathologies.

bestrophin 1 | volume-regulated anion channel | induced pluripotent stem cell | retinal pigment epithelium | mouse sperm

**T**ight regulation of cell volume is fundamental to proper cell function and survival. In general, rapid water influx across cell membranes leads to cell swelling, which in turn activates net efflux of K<sup>+</sup> and Cl<sup>-</sup>, thereby triggering the release of osmotically obligated water from the cell. Essential to this process is the activation of a current primarily carried by chloride ions (I<sub>swell</sub>). This current is gated by volume-regulated anion channels (VRACs) returning the cell to a controlled state of homeostatic integrity, a complex mechanism commonly referred to as regulatory volume decrease (RVD) (1, 2). Although VRACs share common features in almost all cell types, it is unclear whether there is one ubiquitous channel or a diversity of chloride channels with slightly differing functional properties. In this context, three families of proteins—the Ca<sup>2+</sup>- and/or volume-sensitive anoctamins, bestrophins, and the recently discovered LRRC8s—are presently at the center of interest (3–7).

Bestrophin 1 (*BEST1*), a member of the human bestrophin family of four paralogous genes, encodes an integral membrane protein strongly expressed in the human retinal pigment epithelium (RPE) (8). Mutations in *BEST1* have been associated with various macular dystrophies most prominently represented by Best disease (BD), a central retinopathy with autosomal dominant inheritance but variable penetrance and expressivity (9, 10). Key features of BD pathology include a striking lipofuscin accumulation in the macular RPE (11) and an abnormal light peak (LP)/dark trough ratio in the electro-oculogram (EOG) reflective of an impaired RPE

(12). The abnormalities in the LP were suggested to be compatible with a function of BEST1 as a Ca<sup>2+</sup>-activated Cl<sup>-</sup> channel (CaCC) (13, 14).

Addressing BEST1 function, several studies have suggested a role of the protein in distinct basic cellular processes such as Ca<sup>2+</sup> homeostasis, neurotransmitter release, and cell volume regulation. These studies mostly relied on BEST1 overexpression in HEK293 cells or conducted in vitro experiments with isolated cells from existing *Best1*-deficient mouse lines. In summarizing these data, BEST1 was shown to be (i) a calcium sensor localized to the endoplasmic reticulum (ER) of mouse RPE (15), (ii) an intracellular Cl<sup>-</sup> channel activating anoctamin 1 (ANO1) located at the plasma membrane of mouse trachea (5), (iii) a modulator of voltage-gated Ca<sup>2+</sup> channels in murine RPE (16), and (iv) a channel for tonic GABA or slow glutamate release in mouse glia cells and astrocytes (17, 18). To date, the functional role of *Best1* has not been determined in the mouse testis, the site of highest endogenous *Best1* expression in the mouse (19). In addition, using patient-derived hiRPE cells, the role of BEST1 in mediating ER calcium release and/or uptake was shown (20). In contrast, two independent studies in S2R+ cells from *Drosophila melanogaster* strongly suggested the invertebrate *Drosophila Best1* (*dBest1*) to act as a volume-regulated chloride channel but with biophysical characteristics

## Significance

First insight into the molecular identity of volume-regulated anion channel (VRAC) emerged only recently by demonstrating a role for leucine-rich repeats containing 8A (LRRC8A) in channel activity. Our results now expand on VRAC biology, suggesting a model where VRAC subunit composition is cell type- or tissue-specific rather than a single ubiquitous channel formed solely by LRRC8A. Here, we show that bestrophin 1 (BEST1), but not LRRC8A, is crucial in cell volume regulation in retinal pigment epithelium (RPE) cells differentiated from human-induced pluripotent stem cells (hiPSCs). VRAC-mediated currents were strongly reduced in hiPSC-RPE from macular dystrophy patients with pathologic BEST1 mutations. Our model is further supported by in vivo effects of *Best1* deficiency in the mouse that manifest as severe subfertility phenotype due to enhanced abnormal sperm morphology related to impaired volume regulation.

Author contributions: A.M., R.S., K.K., C.H.W., and B.H.F.W. designed research; A.M., C.B., V.M.M., T.J., L.S., P.W., S.Z., and F.H. performed research; C.B., C.M.R., F.H., and H.S. contributed new reagents/analytic tools; A.M., V.M.M., R.S., K.K., C.H.W., and B.H.F.W. analyzed data; and A.M. and B.H.F.W. wrote the paper.

The authors declare no conflict of interest.

This article is a PNAS Direct Submission.

Freely available online through the PNAS open access option.

<sup>1</sup>To whom correspondence should be addressed. Email: bweb@klinik.uni-regensburg.de.

This article contains supporting information online at [www.pnas.org/lookup/suppl/doi:10.1073/pnas.1418840112/-DCSupplemental](http://www.pnas.org/lookup/suppl/doi:10.1073/pnas.1418840112/-DCSupplemental).

clearly distinct from a vertebrate VRAC (3, 21). By small interfering RNA (siRNA)-mediated knockdown of BEST1 in HEK293 cells (6) and mouse Best1 (mBest1) gene disruption in murine peritoneal macrophages (22), two studies could not show a functional effect of BEST1 on  $I_{swell}$ , thus questioning this protein as a candidate for mammalian VRAC in these cell types. Instead, two studies identified the LRRC8A gene as an essential component of a VRAC in various cultured cell lines (6, 7). In these latter studies, the authors propose a scenario where LRRC8A and the isoforms LRRC8B to LRRC8E form variable cell type-specific hexamers, explaining the variability of VRAC properties in different cell types.

Together, the rather disparate reports on BEST1 function underscore the need to further clarify its role in mammalian VRACs. To this end, we focused on two tissues with strong endogenous BEST1 protein expression—namely, human RPE (8) and mouse sperm (19). Major insight into BEST1 function was gained from (i) RPE cell culture models established via hiPSC technology from a healthy donor and two macular dystrophy patients with established pathologic mutations in BEST1 and (ii) a mouse strain deficient for Best1, the murine ortholog of the human BEST1 gene. When exposed to hypo-osmotic challenge, both the mutant hiPSC-RPE cells and Best1-deficient mouse spermatozoa exhibited severe phenotypes, suggesting BEST1 as a crucial component of VRAC function in these cell types. In addition, membrane rupture experiments and voltage-clamp recordings in oocytes from *Xenopus laevis*, coexpressing aquaporin-1 (AQP1) and BEST1 from mouse and human, respectively, demonstrated identical functional properties of the mammalian BEST1 orthologs.

## Results

**Expression Profiling Suggests a Role for BEST1 in Mouse Sperm and Human RPE.** First, we performed RNA and protein expression profiling of Best1 in an extended panel of 14 mouse tissues by RT-PCR and Western blot analysis, respectively. Prominent mRNA expression was almost exclusively restricted to testis, whereas expression in the remaining tissues was weak (e.g., retina, RPE, trachea, lung) or absent (e.g., spleen, liver, colon, kidney) (Fig. 1A and B). This was mirrored by antibody staining of Best1 protein, which was evident only in whole-cell lysates of mouse testis but not in RPE or other tissues analyzed (Fig. 1C and D). Specificity of Best1 polyclonal antibody  $\alpha$ -C45 was vigorously tested and further enhanced by antigen-specific affinity purification (SI Appendix, Fig. S1A–C).

We then explored the ratio of BEST1 expression in RPE relative to testis across phylogeny (Fig. 1B and D). Although humans showed strong BEST1 mRNA expression in RPE and weak expression in testis, an inverse pattern was observed in rat and mouse, whereas in this semiquantitative analysis, pig and rabbit revealed an almost equal ratio of BEST1 transcription in the two tissues. BEST1 antibody staining of RPE and testis in human, pig, and mouse was strong in the RPE of human and pig, whereas the protein was not detectable in the latter species in testis, despite a strong Best1 RNA expression in pig testis (Fig. 1B and D).

To determine gene expression in the transcriptionally silent spermatozoa, we devised an RNA expression assay in the developing testis tissue. Accordingly, increasing expression during

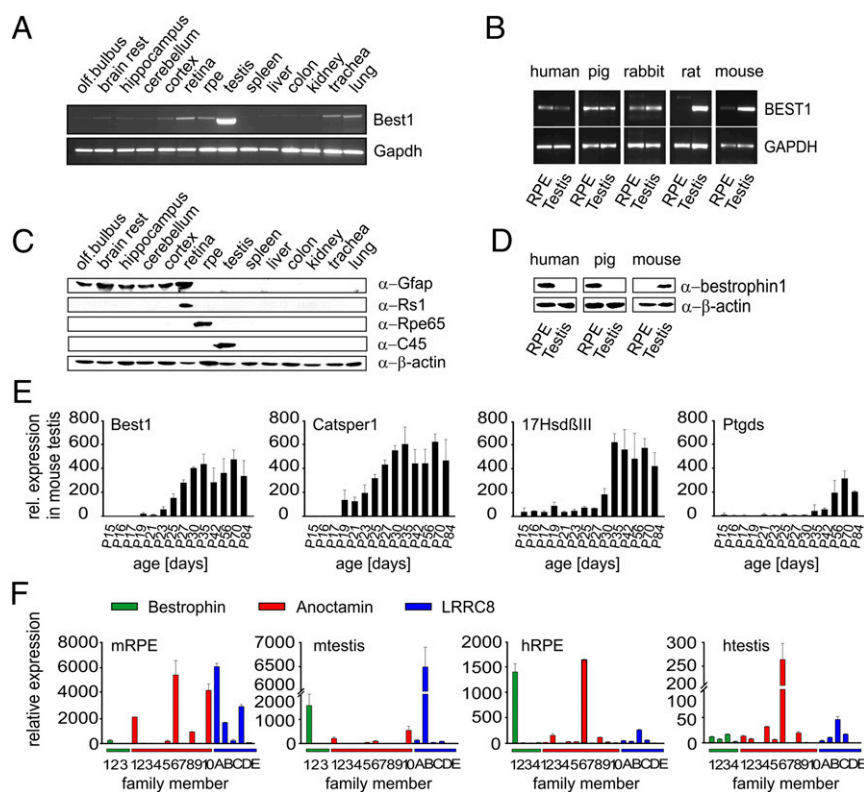


**Fig. 1.** RNA and protein expression analysis of BEST1. (A) RNA expression of BEST1 in 14 mouse tissues and (B) RPE and testis across five mammalian species by RT-PCR. GAPDH served as a control for RNA integrity. For primer sequences, see SI Appendix, Table S5. (C) Western blot analysis in 14 mouse tissues and (D) RPE and testis from human, pig, and mouse using  $\alpha$ -C45 or  $\alpha$ -334 antibody, respectively. Costaining was done with cell-specific markers for glia cells ( $\alpha$ -Gfap), RPE ( $\alpha$ -Rpe65), and retina ( $\alpha$ -Rs1h). Anti-beta actin served as the control. (E) Spatiotemporal RNA gene expression in mouse testis development by quantitative RT-PCR at indicated postnatal time points. Testis samples ( $n = 3$ ) were measured in triplicates to a fixed amount of extracted total RNA. For each sample, the mean  $\pm$  SD is given. (F) Relative mRNA expression of indicated chloride channels in mouse RPE ( $n = 2$ , prepared from 24 eyes), mouse testis ( $n = 3$ ), human RPE ( $n = 2$ ), and human testis ( $n = 3$ ), normalized to Hprt1. For each sample, the mean  $\pm$  SD is given. For primer sequences and Roche library probes, see SI Appendix, Table S7.

testis development should reflect sperm maturation to acquire male fertility. Validation of this assay was carried out for several genes with known transcription profiles in sperm including CatSper1, Cfr, Slx1, Gabra1, and Gabrb3 (Fig. 1E and *SI Appendix, Fig. S2B*) (23–26). Best1 transcripts were first evident at mouse postnatal day (PN) 19, with a strong increase until PN30, where it reached steady-state adulthood levels. This pattern is similar to that of the known sperm-specific Ca<sup>2+</sup> channel CatSper1 but not Leydig/Sertoli cell markers 17βHsdIII and Ptgds (27) (Fig. 1E). Together, these data suggested a sperm-specific expression of Best1.

To define the expression profile of known and putative anion channels in mouse and human RPE and testis, RNA expression was determined for paralogous bestrophin family members, known CaCCs such as the anoctamins, and the recently discovered volume-sensitive LRRC8s (Fig. 1E). Although BEST1 was highly expressed in murine testis and human RPE, expression of BEST2 to BEST4 was similar in testis and RPE from both humans and mice. For the anoctamins, ANO6 consistently showed strong RNA expression in all tissues (see also log<sub>10</sub>-transformed data in *SI Appendix, Fig. S2A*), whereas ANO1 and ANO10 exhibited similar strong expression only in mouse RPE and testis. The remaining anoctamin family members revealed variable but mostly weak expression. For the LRRC8s, high mRNA expression was noted for LRRC8A in mouse RPE and for LRRC8C in the two human tissues and a remarkably strong expression of LRRC8B in murine testis. It is of note that in the developing mouse testis (PN15 to PN84), from the five LRRC8 family members, only LRRC8B showed an RNA expression pattern largely overlapping CatSper1 and Best1 (Fig. 1E and *SI Appendix, Fig. S2B*), arguing for its presence in mouse spermatozoa.

**Best1 Deficiency in the Mouse Impairs Sperm Function and Results in Subfertility.** A gene-targeted knockout mouse was generated (*SI Appendix, Fig. S1 D–F*) and crossed for over 10 generations onto a C57BL/6 (B6) and a CD-1 genetic background, respectively. Offspring from heterozygous (Best1<sup>+/-</sup>) matings of both genetic strains were born at the expected Mendelian ratio of 1:2:1 (*SI Appendix, Table S1*), and Best1<sup>-/-</sup> mice (male and female) developed normally. Initially, the Best1<sup>-/-</sup> mice were evaluated for their ocular phenotype with particular emphasis on retinal and RPE integrity. Analyses included measurement of visual acuity, light and electron microscopy, diurnal RPE phagocytosis, retinal docosahexaenoic acid levels, and basal intracellular Ca<sup>2+</sup> levels of cultured RPE cells but revealed no signs of histological or functional pathology (*SI Appendix, Fig. S3 A–J*). In contrast, male mice deficient for Best1 revealed a severe subfertility phenotype (Table 1), although judged by the presence of vaginal plugs, no differences in the mating behavior of homozygous knockout males versus wild type were noted. Wild-type B6 females that mated with B6 Best1<sup>-/-</sup> males gave birth to only 40% of pups (mean litter size, 4 ± 2.2 pups) compared with wild type (8.5 ± 2.2 pups). Fertility problems were even more pronounced in CD-1 Best1<sup>-/-</sup> males, with only 7 pups born out of 23 intercrosses (0.3 pups per mating), whereas control breedings resulted in an average of 12.1 pups per intercross (Table 1).

We next analyzed mouse Best1 expression in the male reproductive tract by immunolabeling spermatozoa (Fig. 2A) and epididymus (Fig. 2B) with α-C45 antibodies. Immunolabeling consistently stained the equatorial segment of the sperm head in wild-type but not in Best1<sup>-/-</sup> sperm (Fig. 2A). In cell-surface biotinylation experiments, Best1 was identified in the biotin fraction, whereas intracellular tubulin was absent (Fig. 2C), indicating that Best1 is mainly localized to the plasma membrane.

To further characterize the subfertility phenotype, spermatozoa from CD-1 Best1<sup>-/-</sup> males and wild-type littermates was released from the cauda epididymis into media with an osmolality of 290 mmol·kg<sup>-1</sup> (TYH290). In the epididymis, sperm are stored at an osmolality of about 420 mmol·kg<sup>-1</sup>. The release into TYH290 (Δosmolality, -130 mmol·kg<sup>-1</sup>) mimics the osmotic shock that ejaculated sperm experience upon transfer into the female uterine tract (28). Sperm quality parameters such as morphology, acrosome integrity, viability, and motility were assessed (Fig. 2 D–G). By microscopic inspection, a high percentage of heads without tails was noted in the Best1<sup>-/-</sup> sperm population, indicative of enhanced decapitation (Fig. 2D). Strikingly, a large fraction of CD-1 Best1<sup>-/-</sup> sperm displayed severe coiling and angulation of the flagellum—a well-known phenotype referred to as curly tail. The curly-tail phenotype reflects impaired sperm volume regulation (29). In addition, a ~30% decline of viable sperm combined with an increase in the number of acrosome-reacted, -vesiculated, or -thickened acrosomal structures was monitored (Fig. 2 D–F). Consistent with the milder subfertility phenotype of B6 Best1<sup>-/-</sup> males, a high number of spermatozoa from B6 knockouts displayed a thickened acrosome but were less vesiculated and less acrosome-reacted compared with CD-1 Best1<sup>-/-</sup>. Importantly, the fraction of sperm with tail abnormalities was lower in B6 Best1<sup>-/-</sup> spermatozoa (*SI Appendix, Fig. S1G*). In CD-1 Best1<sup>-/-</sup>, the fraction of acrosome intact spermatozoa declined dramatically as the spermatozoa progressed from the caput to the corpus and cauda region of the epididymal duct (Fig. 2F). Finally, sperm motility parameters such as curvilinear velocity (VCL), average path velocity (VAP), straight line velocity (VSL), and amplitude of lateral head displacement (ALH) were analyzed from video recordings, revealing a severe decrease in all motility parameters in CD-1 Best1<sup>-/-</sup> sperm compared with wild type ( $P < 0.001$ ) (Fig. 2G, *SI Appendix, Table S2*, and *Movies S1* and *S2*). Taken together, sperm characteristics of both CD-1 and, to a lesser extent, B6 Best1<sup>-/-</sup> mice suggest that sperm suffer from an impaired volume regulation, similar to studies on analogous morphological abnormalities reported in other knockout mouse models upon cell swelling (30, 31).

**An Impaired Tolerance to Osmotic Change Could Underlie the Sperm Defect in CD-1 Best1<sup>-/-</sup>.** To functionally delineate the subfertility phenotype that, in principle, could be attributed to disturbances in RVD but also to defects in other signaling mechanisms (e.g., Ca<sup>2+</sup> homeostasis), changes in intracellular Ca<sup>2+</sup> concentration ([Ca<sup>2+</sup>]<sub>i</sub>) in CD-1 Best1<sup>-/-</sup> sperm were examined. Sperm were released into TYH420 medium and stimulated by (i) hypotonic swelling in TYH290 medium, (ii) 100 μM ATP, or (iii) 50 μM

**Table 1. Breeding performance of Best1<sup>-/-</sup> and wild-type mice**

| Genetic background | BEST1, genotype of parents |                      | BEST1, offsprings   |                   | <i>P</i> value, Fisher exact <i>t</i> test |
|--------------------|----------------------------|----------------------|---------------------|-------------------|--|
|                    | Males ( <i>n</i> )         | Females ( <i>n</i> ) | Litter ( <i>n</i> ) | Pups ( <i>n</i> ) |  |
| C57BL/6            | +/+ (12)                   | +/+ (35)             | 23                  | 195               | 1,5E-07                                    |
|                    | -/- (12)                   | +/+ (35)             | 19                  | 75                |  |
| CD-1               | +/+ (8)                    | +/+ (23)             | 23                  | 278               | 3,4E-08                                    |
|                    | -/- (8)                    | +/+ (23)             | 4                   | 7                 |  |

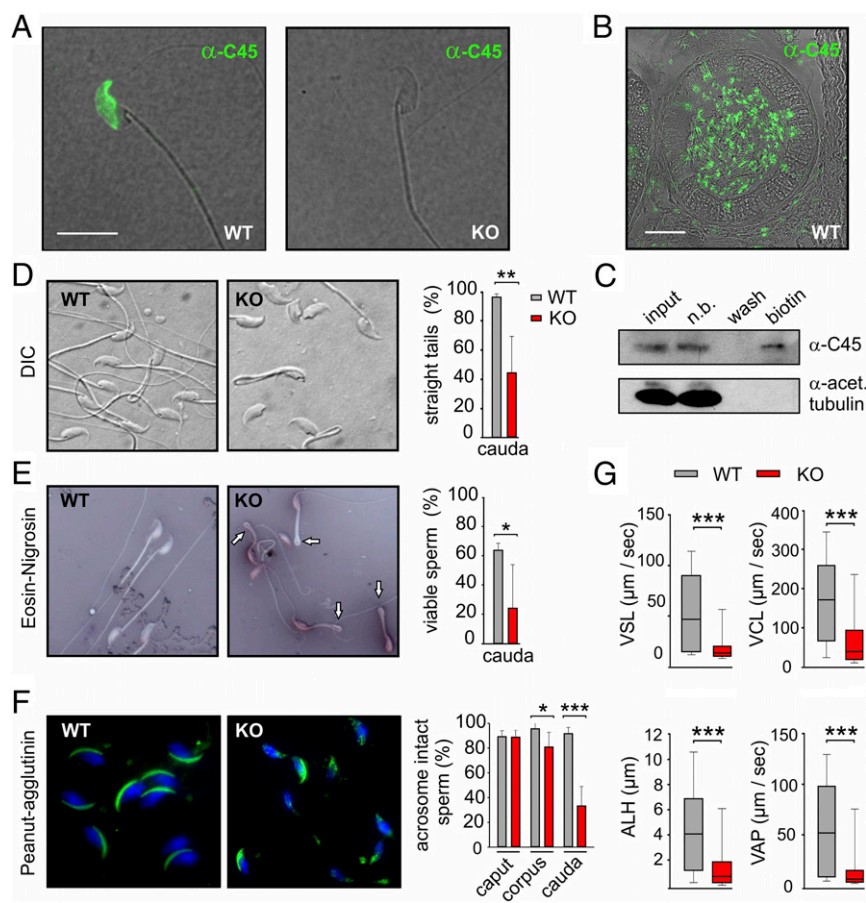


**Fig. 2.** Effects of Best1 deficiency on sperm quality parameters in CD-1 mice. (A) Immunofluorescence staining of spermatozoa from wild-type and Best1<sup>-/-</sup> mice and (B) epididymal cryosection with  $\alpha$ -C45 (also see *SI Appendix, Fig. S1 A–C*). (Scale bar, 10  $\mu$ m and 40  $\mu$ m, respectively.) (C) Spermatozoa from 12 CD-1 male mice were subjected to cell surface biotinylation. Labeled sperm sample was immunoprecipitated with streptavidin, transferred to nylon membranes, and probed as indicated (n.b., unbound fraction). (D) CD-1 Best1<sup>-/-</sup> spermatozoa showing enhanced decapitation and angulated sperm tails. Percentages of straight tails and (E) stained (dead) and colorless (live) spermatozoa from the cauda epididymis after eosin–nigrosin staining from 100 spermatozoa of wild-type ( $n = 10$ ) and CD-1 Best1<sup>-/-</sup> ( $n = 5$ ) mice. (F) CD-1 Best1<sup>-/-</sup> mice showing acrosome-reacted spermatozoa using PNA-488 staining. Percentages of acrosome intact cells (uniform apple green fluorescence) to acrosome-reacted sperm (perforated or absent acrosome cap) from 150 spermatozoa of wild-type ( $n = 16$ ) and Best1<sup>-/-</sup> mice ( $n = 10$ ) of spermatozoa from caput, corpus, and cauda epididymis. (G) Box and Whisker plots of sperm velocity parameters including VSL, VCL, ALH, and VAP. Each box plot shows the interquartile range of 382 spermatozoa from CD-1 wild-type ( $n = 3$ ) and 654 spermatozoa from Best1<sup>-/-</sup> mice ( $n = 7$ ). For further details, see *SI Appendix, Table S2*. Spermatozoa were released into TYH290 media. Values are given as mean  $\pm$  SD. Two-sided Student's *t* test or Wilcoxon signed rank test: \*  $P < 0.05$ ; \*\*  $P < 0.01$ ; \*\*\*  $P < 0.001$ .

cyclopiazonic acid (CPA), a potent inhibitor of calcium ATPase activity. Changes in Ca<sup>2+</sup> levels in sperm heads were recorded as a ratio of fura-2 fluorescence emission upon excitation at 340 nm and 380 nm (Fig. 3A). Before the application of a stimulus, no significant differences in fluorescence ratio were observed, suggesting that basal Ca<sup>2+</sup> levels were similar in wild-type and CD-1 Best1<sup>-/-</sup> sperm (Fig. 3B). Hypotonic swelling in TYH290 evoked a transient Ca<sup>2+</sup> increase. The peak amplitude (Fig. 3C and D) and the recovery rate (Fig. 3E) of the swelling-induced Ca<sup>2+</sup> transient were similar in wild-type and CD-1 Best1<sup>-/-</sup> sperm. Treatment of sperm with 100  $\mu$ M ATP to activate P2X receptors (32) evoked a transient Ca<sup>2+</sup> increase, whose characteristics were similar in wild-type and CD-1 Best1<sup>-/-</sup> mice (Fig. 3D and F), whereas no calcium increase was detected upon 50  $\mu$ M CPA application (*SI Appendix, Fig. S4 A and B*).

To address osmotic tolerance and its possible impairment as the basis for the severe sperm phenotype in CD-1 Best1<sup>-/-</sup> mice, total motility and sperm velocity parameters VAP, VSL, VCL, and ALH were evaluated from caudal spermatozoa. In a time-lapse experiment, caudal spermatozoa were exposed to solutions with increasing osmolalities. The percentage of motile sperm was

relatively stable for up to 2 h within all osmotic solutions, with the possible exception of wild-type sperm at 420 mmol·kg<sup>-1</sup> (Fig. 3G). Although CD-1 Best1<sup>-/-</sup> mice showed a significant lower percentage of motile sperm compared with wild type at all osmotic conditions tested (22  $\pm$  8% vs. 65  $\pm$  7%), statistics on pooled data from the three osmotic conditions revealed a rescue of total motility in spermatozoa from CD-1 Best1<sup>-/-</sup> mice with increasing osmolality (THY290, 16  $\pm$  4%; THY350, 20  $\pm$  7%; THY420, 31  $\pm$  6%) (Fig. 3H and *SI Appendix, Table S2*). Notably, in CD-1 Best1<sup>-/-</sup> mice, the percentages of motile spermatozoa reflected the number of viable cells (Fig. 2E), indicating that those sperm that are alive are motile. From these data, we conclude that the lack of Best1 in mouse spermatozoa does not affect Ca<sup>2+</sup> homeostasis but rather renders sperm unable to cope with changes in osmotic pressure.

**Cell Swelling Activates Identical Currents in *X. laevis* Oocytes Expressing Human and Mouse BEST1.** Next, we explored whether BEST1 function is evolutionarily conserved between mouse and man. To this end, *X. laevis* oocytes were exposed to a hypotonic bath solution that induced cell swelling and rupture of the oocyte membrane in

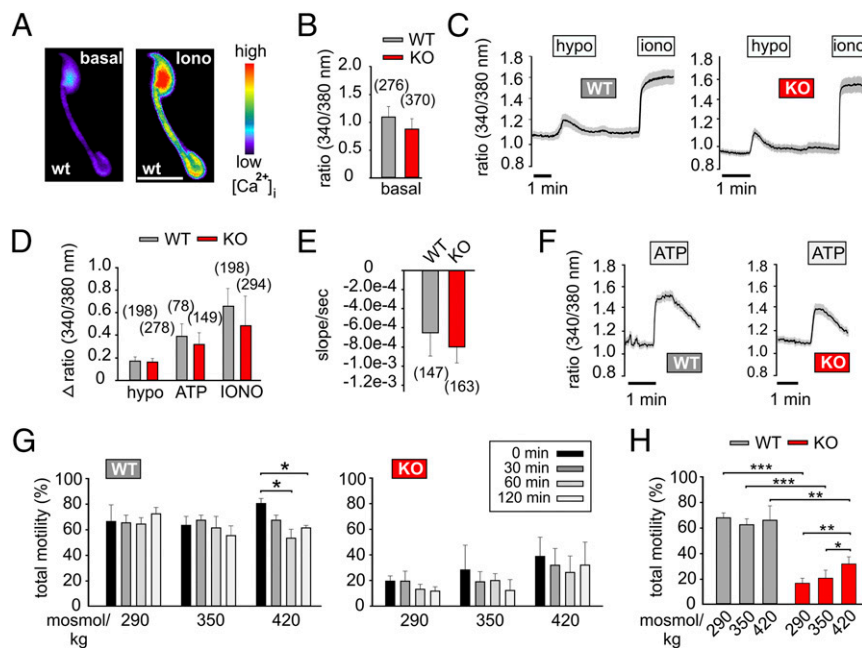


**Fig. 3.** Consequences of Best1 deficiency on calcium signaling and osmotic tolerance in mouse sperm. (A–F)  $\text{Ca}^{2+}$  imaging in the sperm head from spermatozoa of corpus epididymis from CD-1 wild-type and CD-1 Best1<sup>-/-</sup> mice ( $n = 3$ –6) released into TYH420 media. (A) Representative images of cytosolic  $\text{Ca}^{2+}$  levels  $[\text{Ca}^{2+}]_i$  in mouse sperm unstimulated (Left) or upon ionomycin application (Right). The pseudocolor image shows the  $[\text{Ca}^{2+}]_i$  increase in sperm head. (B) Bar graphs showing basal  $[\text{Ca}^{2+}]_i$  levels. (C) Averaged graphs of  $[\text{Ca}^{2+}]_i$  increase upon hypotonic stimulation. (D) Summary of basal  $[\text{Ca}^{2+}]_i$  levels, ATP-induced, and swelling-activated increases in  $[\text{Ca}^{2+}]_i$  obtained from experiments shown in B, C, and F. Ionomycin was used for determination of maximum  $[\text{Ca}^{2+}]_i$ . Black lines indicate the averaged responses of at least 30 spermatozoa; gray area indicates SEM. Also see *SI Appendix, Fig. S4*. (E) Bar graphs showing recovery rates (slope $\cdot$ s<sup>-1</sup>) from swelling-induced  $[\text{Ca}^{2+}]_i$  maximum peak to initial levels. (F) Averaged graphs of  $[\text{Ca}^{2+}]_i$  increase in response to 100  $\mu\text{M}$  ATP. (G) Percentages of total sperm motility from caudal spermatozoa of three CD-1 wild-type and seven Best1<sup>-/-</sup> mice exposed to defined osmotic conditions. Recordings were taken at indicated time points after initial exposure to TYH290, TYH350, or TYH420 media. (H) Summary of G. Mean values were pooled for the three indicated osmotic conditions. For further details, see *SI Appendix, Table S2*. Values are given as mean  $\pm$  SEM. Two-sided unpaired Student's *t* test: \*  $P < 0.05$ ; \*\*  $P < 0.01$ ; \*\*\*  $P < 0.005$ . *n*, number of spermatozoa.

cells expressing the water channel aquaporin 1 (AQP1) (Fig. 4A). Cell swelling and rupture of the oocyte membrane was significantly delayed in oocytes coexpressing human BEST1 or mouse Best1 (Fig. 4B). In contrast, expression of mutant proteins BEST1-R218C and BEST1-Y227N did not delay oocyte bursting (Fig. 4B). Notably, 50% of the oocytes expressing AQP1, AQP1/R218C, and AQP1/Y227N burst within the first 30 s ( $T_{50} = 0.25$  min, 0.4 min, and 0.25 min, respectively), whereas expression of human BEST1 or mouse Best1 significantly increased  $T_{50}$  to 2.5 min and 4.5 min, respectively (Fig. 4B and C).

We then examined whether hypotonic cell swelling in the presence of BEST1 also activates membrane currents in *X. laevis* oocytes. Defolliculated oocytes were thoroughly monitored for endogenous swelling-activated whole-cell currents as reported earlier (33). Three days after injection, oocyte rupture and volume-activated whole-cell currents were virtually absent in water-injected control oocytes, similar to earlier studies (34). In AQP1-injected oocytes, the hypotonic bath solution activated only a small endogenous whole-cell current before membrane bursting (Fig. 4D and E). In AQP1/hBEST1 and AQP1/mBest1 coexpressing cells, the volume-activated currents were twice as large as in control oocytes expressing AQP1 only (Fig. 4D–G). The swelling-activated current was inhibited by 200  $\mu\text{M}$  dihydro-4,4'-diisothiocyanostilbene-2,2'-disulphonic acid (DIDS) (inhibition by  $48 \pm 7.9\%$ ;  $n = 5$ ) but not by other known CaCC blockers, such as 5-nitro-2-(phenylpropylamino)-benzoate (NPPB) (50  $\mu\text{M}$ ) (inhibition by  $9 \pm 1.1\%$ ;  $n = 5$ ) or CaCCinh-AO1 (20  $\mu\text{M}$ ) (inhibition by  $3 \pm 0.4\%$ ;  $n = 4$ ) (35, 36). Notably, volume-activated whole-cell currents in AQP1/hBEST1 and AQP1/mBest1 coexpressing cells were rather linear and showed only little time-dependent inactivation, as reported earlier (21, 34). Together,

these experiments suggest that human and mouse BEST1 are both activated by cell swelling, thereby leading to RVD and delay in hypotonic cell rupture. The disease-associated BEST1 mutations—BEST1-R218C, BEST1-Y227N, BEST1-Q238R, and BEST1-A243V—abolished ion channel function (Fig. 4B, C, and G). In addition, coexpression of AQP1/hBEST1 and BEST1-A243V also leads to significant reduction in VRAC currents, in agreement with a dominant-negative mode of action of BEST1 mutations on wild-type BEST1, as suggested earlier (37).

**hiRPE Cells from Two Macular Dystrophy Patients Reveal Aberrant BEST1 Localization.** To analyze functional aspects of BEST1 in human RPE, we resorted to RPE differentiated from human-induced pluripotent stem cells. Such cell lines reveal properties largely overlapping those of native cells (38) and were generated from a healthy donor and two macular dystrophy patients harboring the heterozygous mutations BEST1-A243V and BEST1-Q238R, respectively (*SI Appendix, Fig. S5 A–F*). Upon visual inspection, the three cell lines were morphologically identical, all revealing a hexagonal cell shape and strong pigmentation, unique features of differentiated RPE cells (Fig. 5A). Epithelial integrity of the hiRPE cells was established by measuring trans-epithelial resistance (TER) with a mean TER of  $241 \pm 57 \Omega\cdot\text{cm}^2$  for the three cell lines after correction for background.

Immunostaining of control hiRPE cells with  $\alpha$ -334 BEST1 antibody confirmed correct protein localization to the basolateral plasma membrane relative to  $\alpha$ -ZO-1, a tight junction marker localized at the apical side of RPE cell clusters (Fig. 5B). In contrast, BEST1-A243V cells revealed localization of BEST1 to both the plasma membrane and the cytoplasm, whereas in BEST1-Q238R, the mutant protein appeared grossly reduced

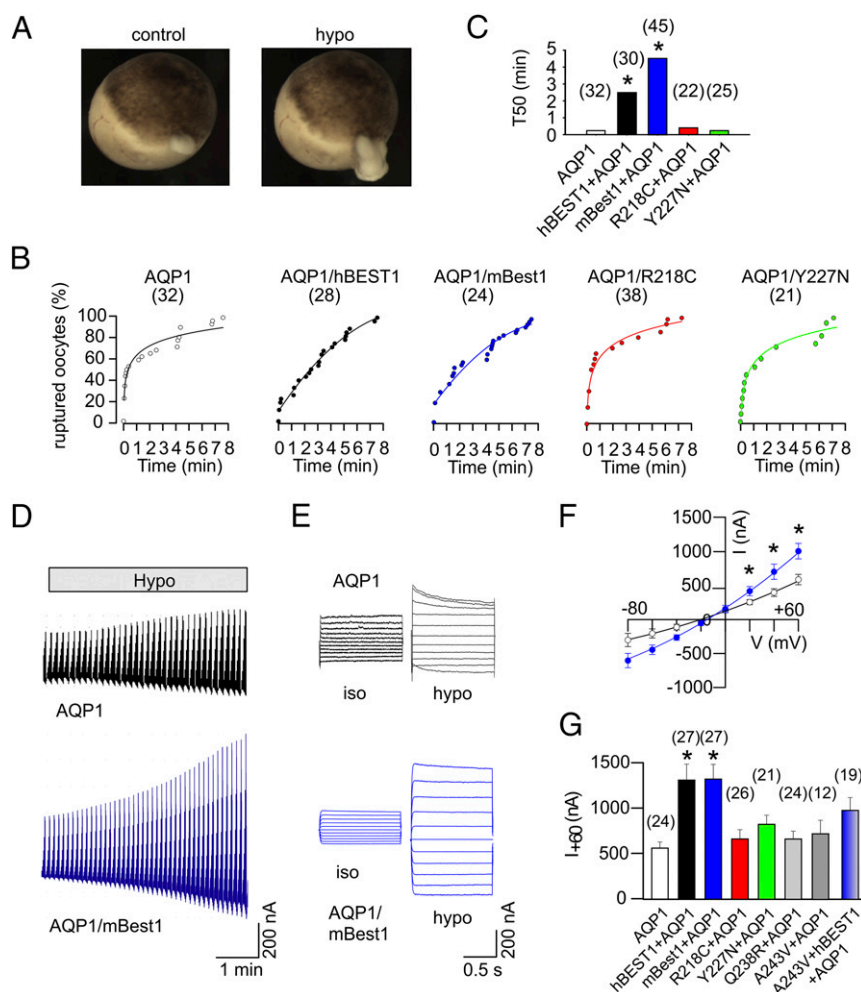


**Fig. 4.** Rescue of swelling-induced membrane rupture of AQP1-expressing *X. laevis* oocytes by coexpression of hBEST1 or mBest1. (A) Photomicrograph showing two *X. laevis* oocytes under hypotonic condition injected with water as the control (Left) or AQP1 (Right). (B) Cumulative plot of ruptured *X. laevis* oocytes, coexpressing AQP1 and the indicated BEST1 constructs in a time course of 0–8 min after exposure to hypotonic media. Data were plotted as colored circles and fitted by double-exponential regression. (C) Bar graph summarizing B. T50, time to burst with 50% of the total number of oocytes indicated. (D–F) Voltage-clamp recordings of *X. laevis* oocytes, expressing AQP1 (black) or AQP1/mBest1 (blue). (D) Kinetic of swelling-induced anion currents ( $I_{\text{swell}}$ ) at  $-80$  and  $+60$  mV over time. (E) Current traces in response to voltage steps (20 mV intervals from  $-0$  to  $+60$  mV) in isotonic solution ( $290 \text{ mmol}\cdot\text{kg}^{-1}$ ) and after 5 min in hypotonic solution ( $200 \text{ mmol}\cdot\text{kg}^{-1}$ ). (F) Current–voltage relationship under hypo-osmotic conditions. (G) Summary of  $I_{\text{swell}}$  from oocytes, coexpressing AQP1 and the indicated BEST1 constructs at  $+60$  mV. AQP1-expressing oocytes served as control. Values are given as mean  $\pm$  SEM; n, number of measured cells. An asterisk indicates significant differences compared with AQP1-expressing oocytes (two-sided unpaired Student's *t* test,  $* P < 0.05$ ). Defolliculated oocytes were carefully monitored for endogenous  $I_{\text{swell}}$  before experiments.

compared with normal RPE and to an even larger extent localized within the cytoplasm with only minor staining of the plasma membrane (Fig. 5B). These findings supported a dominant-negative effect of the mutant protein on wild-type BEST1. Semiquantitative Western blot analysis confirmed reduced expression of BEST1 protein in BEST1-Q238R, whereas RNA expression levels appeared similar in the three cell lines analyzed (Fig. 5C and D).

We further tested RNA expression for bestrophins, known CaCCs, and volume-sensitive LRRC8s and confirmed that the profiles are similar for the three hiRPE cell lines compared with native RPE (Figs. 1F and 5E, and SI Appendix, Fig. S5G), suggesting that the hiRPE cell lines represent suitable cellular models to investigate BEST1 function in a setting similar to native RPE.

**Swelling-Induced Anion Currents Are Absent in hiRPE Cells from Macular Dystrophy Patients with Heterozygous BEST1 Mutations.** To characterize swelling-induced currents in hiRPE cells, whole-cell voltage-clamp recordings were performed in isosmotic bath solution (intra- and extracellular solution at  $290 \text{ mmol}\cdot\text{kg}^{-1}$ )

(SI Appendix, Fig. S6A). First, wild-type hiRPE cells [ $(+/+)$ ,  $n = 18$ ] were challenged by exchanging the extracellular bath for a hyposmotic solution ( $260 \text{ mmol}\cdot\text{kg}^{-1}$ ). The resulting difference in osmotic pressure led to an increase in conductance, as monitored by increased inward and outward currents in response to voltage ramps (Fig. 6A and B). Functional properties of this current were analyzed in a subset of cells ( $n = 7$ ) using an extended protocol. Under the given ionic conditions, currents were slightly outward rectifying and reversed polarity at  $4 \pm 2$  mV (Fig. 6C and SI Appendix, Fig. S6B). The osmotic pressure-induced currents increased with a half time of  $3.3 \pm 0.2$  min (SI Appendix, Fig. S6B) to reach a plateau on average of  $2.3 \pm 0.7$  nA (Fig. 6D). Reducing the extracellular  $\text{Cl}^-$  concentration to 2 mM by replacing  $\text{Cl}^-$  with gluconate led to a marked decrease of outward currents to  $0.6 \pm 0.2$  nA (compatible with a diminished influx of anions due to a lower permeability for gluconate compared with  $\text{Cl}^-$ ) (Fig. 6A and D), paralleled by a shift of the reversal potential to positive values ( $22 \pm 6$  mV) (Fig. 6C). This indicates that the swelling-activated current is carried by anions.

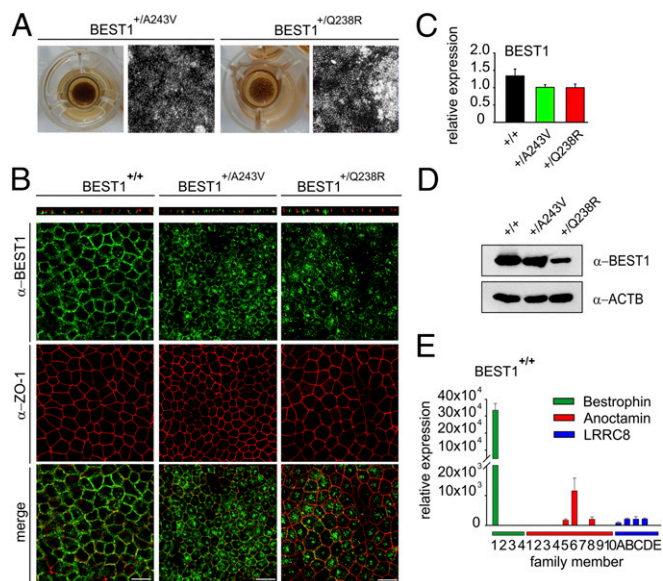


**Fig. 5.** Expression and localization of normal and macular dystrophy-associated mutant BEST1 in hiRPE cells. (A) Images of hiRPE cells from two BD patients (+A243V or +Q238R) after 2 mo grown on 12-well-transwell filters (Left). Bright-field microscopy of pigmented hiRPE cells (Right). (Scale bar, 100  $\mu$ m.) (B) Flat mount immunofluorescence imaging of BEST1 and ZO-1 proteins. Shown are *x-y* and *x-z* projections of confocal image stacks. (Scale bars, 20  $\mu$ m.) (C) Quantification of BEST1 RNA expression by quantitative RT-PCR of total RNA extracted from hiRPE transwell filters. Samples were performed in triplicates and normalized to HPRT1. (D) Western blot analysis of hiRPE cell lysates using BEST1 antibody  $\alpha$ -334 for detection. Beta-actin (ACTB) served as the loading control. (E) Relative mRNA expression of indicated genes in hiRPE cells from a healthy donor (BEST1<sup>+/+</sup>) ( $n = 3$ ) normalized to HPRT1. For results from patient-derived RPE cells, see *SI Appendix, Fig. S5G*. Primer sequences and Roche library probes are given in *SI Appendix, Table S7*.

Moreover, adding the nonspecific chloride channel inhibitor DIDS (300–600  $\mu$ M) to the external bath solution also markedly reduced currents, by stronger affecting outward currents (Fig. 6 *A*, *C*, and *D*), pointing to an anion-permeable pore that conducts the swelling-induced current in hiRPE (<sup>+/+</sup>) cells.

Additionally, osmotic pressure-induced  $I_{swell}$  in hiRPE (<sup>+/+</sup>) cells featured a characteristic time- and voltage-dependent inactivation at strong positive voltages (Fig. 7 *A* and *B*). After activation of  $I_{swell}$  by application of a hyposmotic bath solution, currents showed pronounced current relaxation (inactivation) during a depolarizing voltage step (120 mV, 1 s) with a decay following a double-exponential time course (time constant  $\tau_1 = 0.22 \pm 0.13$  s and  $\tau_2 = 0.9 \pm 0.15$  s). Currents recovered from inactivation at negative voltages (–60 mV) with a time constant of  $\tau = 1.57$  s. The time- and voltage-dependent inactivation can be modulated by extracellular cations (39) and is absent in extracellular  $Ca^{2+}$ -free bath solution (Fig. 7*C*), whereas the activation of  $I_{swell}$  remained unaffected (Fig. 7*D*). Together, these data argue for the presence of an  $I_{swell}$  in hiRPE (<sup>+/+</sup>) cells that exhibits the functional properties of a typical VRAC (2).

hiRPE cells from BD patients carrying mutations BEST1-A243V or BEST1-Q238R, respectively, showed voltage-driven currents under isosmotic conditions that were similar (BEST1-A243V) or slightly smaller (BEST1-Q238R) compared with hiRPE (<sup>+/+</sup>) cells (Fig. 6*B* and *SI Appendix, Table S3*). Notably, challenging the cells with a hyposmotic bath solution induced only small voltage-driven currents (Fig. 6*A–D* and *SI Appendix, Fig. S6 C and D* and *Tables S3 and S4*) in a fraction of cells (8 out of 22 in BEST1-Q238R and 6 out of 14 cells in BEST1-A243V). The remaining cells did not significantly change conductance upon

treatment with a hypotonic solution. The residual currents in responsive cells were still sensitive to the application of low  $Cl^-$ -containing solution or DIDS (Fig. 6*A* and *D*). However, currents induced by depolarizing voltage steps during hypotonic challenge did not show any inactivation or current relaxation, similar to the situation found under isosmotic conditions (*SI Appendix, Fig. S6 E–H*).

**Stable Knockdown of LRRC8A in hiRPE Cells Has No Effect on  $I_{swell}$ .** Motivated by two recent publications that identified LRRC8A as an essential component of VRACs in several cell lines (6, 7), we analyzed a potential role of LRRC8A in hiRPE volume regulation. We therefore established a stable short-hairpin RNA (shRNA)-mediated knockdown of LRRC8A expression in hiRPE cells of healthy control. After two rounds of lentiviral transduction with shRNA against LRRC8A (hiRPE<sub>shLRRC8A</sub>), quantitative RT-PCR analysis revealed a 76% mRNA decrease of LRRC8A expression compared with control cells treated with lentivirus coding for scrambled RNA (hiRPE<sub>scramble</sub>) (Fig. 8*A*). This was confirmed by antibody staining of LRRC8A, which was markedly reduced in whole-cell lysates of hiRPE<sub>shLRRC8A</sub> cells (Fig. 8*B*). A standardized protocol of hypotonic current activation and subsequent isotonic inactivation was used for whole-cell voltage-clamp recordings (Fig. 8*C*). Challenging the cells with hypo-osmotic bath solution led to activation of  $I_{swell}$  in 54% of hiRPE<sub>shLRRC8A</sub> (27/50 cells) and in 40% of the hiRPE<sub>scramble</sub> (25/63 cells) cells, whereas the average magnitude of  $I_{swell}$  in hiRPE<sub>shLRRC8A</sub> cells was somewhat larger compared with hiRPE<sub>scramble</sub> controls (outward, 150%,  $P = 0.03$ ; inward, 150%,  $P = 0.3$ , n.s.) (Fig. 8*D*). Taken together, the shRNA-mediated knockdown of LRRC8A in hiRPE cells led to a reduction in both the level of LRRC8A mRNA and protein, whereas no significant difference in  $I_{swell}$  between hiRPE<sub>shLRRC8A</sub> and hiRPE<sub>scramble</sub> was observed (neither in number of responders nor in magnitude of current).

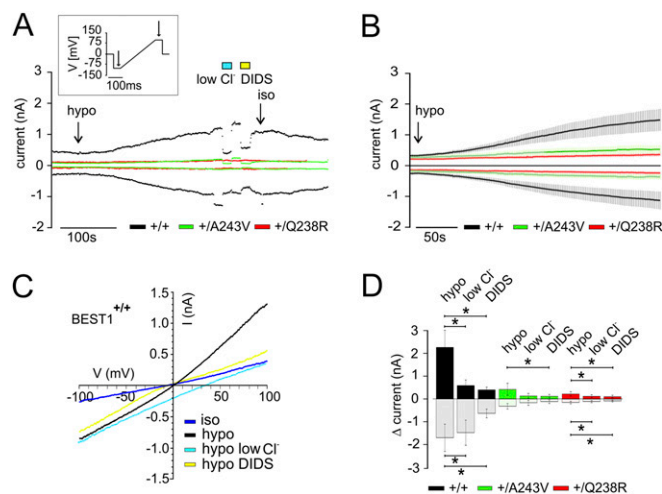


**Fig. 6.** Swelling-induced anion currents in hiRPE cells are greatly reduced in patients with macular dystrophy. (A–D) Whole-cell voltage-clamp recordings of hiRPE cells from a healthy donor (<sup>+/+</sup>) and two macular dystrophy patients (+A243V or +Q238R) under indicated conditions. (A) Activation of endogenous anion currents upon hypotonic challenge (260 mmol·kg<sup>-1</sup>) over time. Data were extracted from recordings of voltage ramps at –100 and 100 mV. (B) Averaged currents recorded at –100 to 100 mV upon hypotonic challenge for 5 min. (C) IV plot of selected recordings from A. Also see *SI Appendix, Fig. S6 C and D*. (D) Statistical analysis of  $I_{swell}$  obtained from A–C. Data points are corrected for baseline currents under isotonic conditions (290 mmol·kg<sup>-1</sup>). Values are given as mean  $\pm$  SEM. Two-sided paired Student's *t* test: \*  $P < 0.05$ .

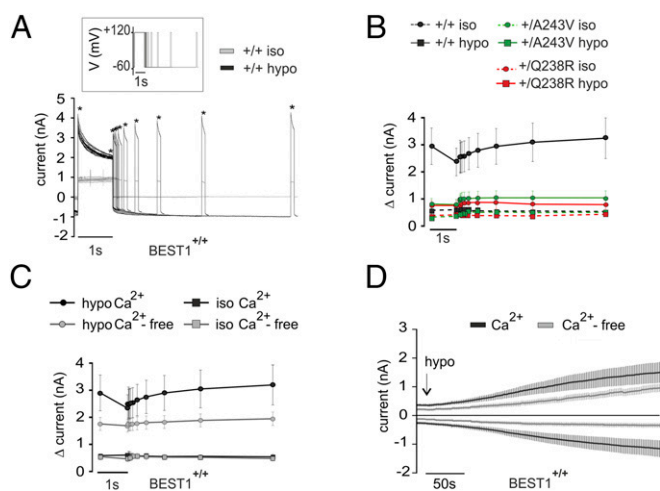


**Fig. 7.** Swelling-induced anion currents in hiRPE cells display time- and voltage-dependent inactivation. (A–D) Voltage-dependent inactivation and recovery from inactivation of  $I_{\text{swell}}$  during a two voltage step experiment. After inactivation of  $I_{\text{swell}}$  during the first voltage step to 120 mV for 1 s, the cell was held at –60 mV with increasing time intervals and then stepped back to 120 mV. (A) Representative recording from the control (BEST1<sup>+/+</sup>). Asterisks indicate time points of current amplitudes analyzed in B and C. (B) Summary of experiments from hiRPE cells of control and BD patients. Also see *SI Appendix, Fig. S6 E–H*. (C) Kinetics of  $I_{\text{swell}}$  (at –100 mV and 100 mV) in hiRPE cells (BEST1<sup>+/+</sup>) under the Ca<sup>2+</sup> conditions indicated. A 1-s depolarizing prepulse led to voltage-dependent inactivation. A second pulse with varying delay revealed time-dependent recovery from inactivation. (D) Summary of voltage-dependent inactivation and time-dependent recovery from inactivation of  $I_{\text{swell}}$  in two-pulse experiments in hiRPE cells (BEST1<sup>+/+</sup>) under the Ca<sup>2+</sup> conditions indicated. The currents are corrected for baseline. Values are given as mean  $\pm$  SEM.

## Discussion

The present study provides several lines of direct and indirect evidence arguing for BEST1 as a crucial component of VRACs in mouse sperm and human RPE. Our findings show that lack or dysfunction of these properties has vital implications on both mouse sperm, resulting in a severe subfertility phenotype, and human RPE cells, strongly reducing swelling-induced anion currents. Moreover, heterologous overexpression of both human and mouse BEST1 in AQP1-coexpressing *X. laevis* oocytes results in a significant rescue in a membrane rupture assay and an increase of  $I_{\text{swell}}$  upon hypotonic stimulation. Importantly, the latter set of experiments demonstrates that mouse and human BEST1 have a similar if not identical role in volume regulation, despite the fact that the two ortholog proteins operate in highly diverse and specialized cell types.

Until now, the mammalian bestrophins and their functional role in classical VRAC activity were rather controversial. Essentially, three main arguments were brought forward. Strikingly, BEST1 whole-cell currents behaved largely insensitive toward hypotonic challenges after heterologous overexpression of bestrophin family members in HEK293 cells (4). We argue that the HEK293 cell system is ill-suited for addressing this particular question, as these cells are known to retain a large proportion of overexpressed BEST1 protein intracellularly (40). Upon hypotonic stimulation, the simultaneous activation of the endogenous LRRC8A-mediated VRAC current in HEK293 cells (6, 7) renders it impossible to distinguish endogenous VRACs from heterologously expressed BEST1 currents. To avoid these methodological difficulties, we resorted to *Xenopus* oocytes, a polarized cell system that provides an important precondition for plasma membrane localization of BEST1 (41). After manual defolliculation and careful monitoring of each single batch for endogenous swelling-

activated whole-cell currents, we recorded BEST1-mediated swelling-sensitive currents that were significantly enlarged relative to endogenous  $I_{\text{swell}}$ . Together, these experiments demonstrated that (i) mouse and human BEST1 are functionally interchangeable and (ii) BEST1 current indeed is activated by hypo-osmotic solution.

Second, the *Drosophila* dBest1 was suggested as a VRAC (3, 21), but the biophysical characteristics of endogenous dBest1 in S2R+ cells from *Drosophila* differed significantly from properties of  $I_{\text{swell}}$  in mammalian VRACs (2). This further questioned the role of mammalian BEST1 as a VRAC, although the discrepant channel characteristics may best be explained by an obvious sequence diversity of bestrophins from arthropod to vertebrate. Specifically, dBest1 reveals a sequence identity to human paralogs BEST1, BEST2, BEST3, and BEST4 of 52%, 53%, 51%, and 49%, respectively. On the basis of such close sequence identities, a human ortholog to *Drosophila* dBest1 cannot be assigned, which makes it rather difficult to compare functional aspects between the phylogenetically related bestrophin families.

Further arguments contradicting a role of BEST1 as a VRAC developed from findings in a knockout mouse model demonstrating that Best1 deficiency failed to eliminate VRACs in peritoneal macrophages (22). Additionally, siRNA-mediated knockdown of endogenous BEST1 in HEK293 cells had no effect on hypotonicity-induced YFP quenching responses (6). These findings, however, do not contradict the results presented in the present study. In fact, no or very weak RNA and protein expression is not in favor of a functional role of mBest1 in macrophages or hBEST1 in HEK293 cells, further supporting our hypothesis of cell- or tissue-specific VRAC channel diversity.

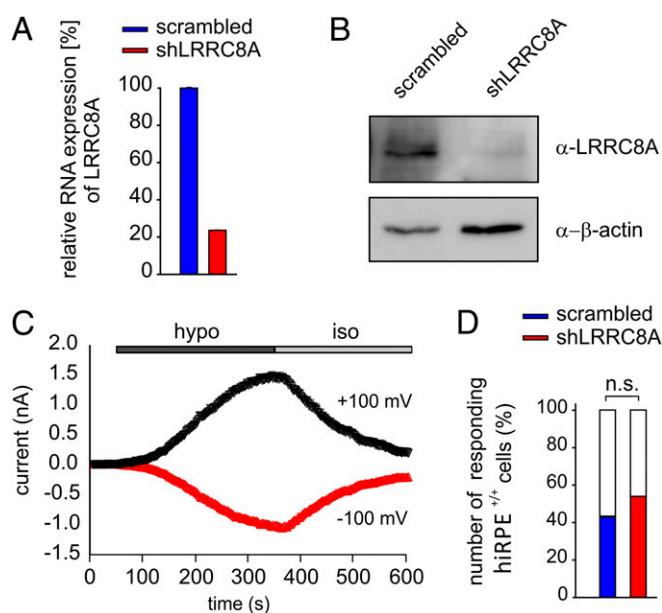


**Fig. 8.** Stable knockdown of LRRC8A in hiRPE cells has no effect on  $I_{\text{swell}}$ . (A) Relative mRNA expression of hLRRC8A in hiRPE<sup>+/+</sup> cells virally transduced with scrambled (hiRPE<sub>scrambled</sub>) and LRRC8A shRNA (hiRPE<sub>shLRRC8A</sub>), normalized to Hprt1 expression ( $n = 2$ , pooled data from analysis after 1 and 4 wk of lentiviral transduction; mean  $\pm$  SD). (B) Western blot analysis of hiRPE<sub>scrambled</sub> and hiRPE<sub>shLRRC8A</sub> lysates using  $\alpha$ -LRRC8A. Per lane, three 12-well-transwell filters were pooled. Anti-beta actin served as the control. (C) Representative graph showing swelling-induced whole-cell currents of a hiRPE<sub>scrambled</sub> cell using a standardized protocol with current activation at 260 mmol·kg<sup>-1</sup> for 300 s and inactivation at 290 mmol·kg<sup>-1</sup> for at least 200 s. Data were extracted from recordings of voltage ramps at –100 and 100 mV. (D) Bar graph depicting the fraction of responders versus nonresponders of analyzed hiRPE<sub>scrambled</sub> ( $n = 63$ ) and hiRPE<sub>shLRRC8A</sub> ( $n = 50$ ) cells.

Although mutations in the *BEST1* gene cause an ocular phenotype in human, our thorough analysis of a Best1-deficient mouse has not revealed a comparable retinal pathology in the murine model. This is in agreement with the lack of Best1 expression in the murine RPE and findings in an independent *Best1*<sup>-/-</sup> knock-out mouse revealing no effect on RPE chloride conductance (16). Conversely, high expression of Best1 in mouse sperm is associated with a strong fertility phenotype. Unfortunately, our evidence linking the observed sperm phenotype to a defect in volume regulation is rather indirect and is not based on direct measurements of ion currents. Particularly for mouse sperm, the latter experimental approach is the most challenging, due to the low volume of sperm cytoplasm and the fact that the plasma membrane of intact spermatozoa is extremely rigid (42). In our hands, shifting to a hypotonic solution repeatedly resulted in loss of the whole-cell configuration between the patch-clamp pipette and the cytoplasmic droplet membrane of the sperm tail. We also tested optical methods to study sperm ion channels via fluorescent indicators. Specifically, we used fluorescent chloride indicator N-(ethoxycarbonylmethyl)-6-methoxyquinolinium bromide (MQAE) and the volumetric indicator Calcein-AM. Again, the results were only a little encouraging due to the miniscule volume of the sperm cytoplasm and the resulting weak fluorescence.

Unexpectedly, sperm motility of *Best1*<sup>-/-</sup> mice was not fully rescued by the hypertonic solution, in contrast to reports, for example, for spermatozoa from the *Slo*<sup>-/-</sup> mouse (43). As suggested by Voets et al. (44), this finding may be explained by VRAC activation in *Best1*<sup>-/-</sup> spermatozoa before ejaculation and could be triggered by reduced intracellular ionic strength. As spermatozoa pass from the testis to the cauda of the epididymis, before ejaculation they are stored in a concentrated environment of high osmolality and low intracellular ionic strength compared with the testicular environment (45). Upon ejaculation, the hypotonic environment of the female tract could still enhance an epididymal *Best1*<sup>-/-</sup> sperm defect, which would then be reflected by the significantly reduced motility compared with the higher osmotic condition.

Recently, LRRC8A was suggested as an integral component of VRAC or, alternatively, crucial for its activation, as shown in siRNA-mediated knockdown and CRISPR/Cas9 genome editing experiments (6, 7). In this model, VRAC is formed by LRRC8 hexamers of LRRC8A and at least one other family member. Hence, small variations of biophysical and biochemical features of VRAC in different cell types (2) may be explained by a variable cell type- or tissue-specific combination of LRRC8A with different LRRC8 isoforms (7). Our findings are not in support of such a model, which is exclusively based on LRRC8A and its family members as the sole components of VRAC. We show that in mouse sperm, only LRRC8B but no other LRRC8 isoform is sufficiently expressed to account for a crucial functional role in this cell type. Considering that disruption or overexpression of isoform LRRC8B alone did not alter  $I_{\text{swell}}$  in HEK293 and HCT116 cells (7), a sole function of LRRC8B appears insufficient to mediate VRAC pore properties in mouse sperm. Furthermore, our data demonstrate that hiRPE cells are well capable of regulating cell volume, although LRRC8A is significantly reduced in our shRNA knockdown experiments.

In conclusion, the identification of BEST1 as an essential component of VRAC in human RPE and the restricted expression of the protein in human RPE and mouse sperm led us to propose a model scenario where VRAC is a cell type- or tissue-specific complex rather than a single ubiquitous channel. A refined knowledge about protein expression in the different cell types and species might help in finding additional components of the vertebrate family of VRACs. Particularly, other members of the bestrophins family need to be assessed for their possible role in volume regulation in specifically defined cells or tissues. Together, our findings provide the basis to further explore the mechanisms of cell volume regulation in normal and diseased

cell physiology, possibly delineating novel therapeutic treatment strategies for BEST1- and other VRAC-associated pathologies.

## Materials and Methods

**Research Involving Humans and Vertebrate Animals.** Experiments involving humans obtained approval of the local ethics review board (University of Regensburg, Germany, Reference No. 11-101-0228). Informed consent was given by each proband participating in the study. Research involving mice and *Xenopus laevis* were conducted in accordance with the German Animal Welfare Act.

**Antibodies.** Antibodies were generated against murine Best1 peptide PESP-TEHLQRRRLDQMSTNIQALMKEHAESYPYRDEAGTKPVLVE (anti-C45) and human BEST1 (amino acid 572 to 585, NP\_004174.1). Additional antibodies: Gfap (#G9269; Sigma-Aldrich), zonula occludens 1 (Invitrogen), LRRC8A (#HPA016811; Sigma-Aldrich), GST (#G7781; Sigma-Aldrich),  $\beta$ -actin (#5441; Sigma-Aldrich), Rpe65 (ab13826; Abcam), acetylated tubulin (#T6793; Sigma-Aldrich) and Rs1 (RS1-3R10) (kindly provided by R. S. Molday, University of British Columbia, Vancouver).

**Mice.** *Best1*-deficient mice were generated as described in *SI Materials and Methods*.

**RNA and Protein Expression.** Expression of BEST1 was analyzed in RPE and testis across different mammalian species. To enzymatically isolate RPE cells, mouse eyecups were transferred to 3 mM L-cysteine in PBS/1 mM EDTA, 1 U/ml papain, and 1 mg/ml BSA. Total RNA was extracted with the RNeasy Mini Kit (Qiagen) and first strand cDNAs were obtained with the RevertAid H Minus First Strand cDNA Synthesis Kit (Fermentas). For RT-PCR reactions, 50 ng of cDNA was used as templates for PCR with Go Taq Polymerase (Promega). Primer sequences are listed in *SI Appendix, Table S5*. For quantitative RT-PCR, primer sequences for amplification of target genes and Roche Library Probes are listed in *SI Appendix, Table S7*. Northern blot analysis was performed as described earlier (9). Total protein extracts were prepared by homogenization in 1  $\times$  PBS supplemented with 1  $\times$  protease inhibitor cocktail (Roche). Protein samples were separated by SDS-polyacrylamide gel electrophoresis and subsequently transferred onto polyvinylidene difluoride membranes (Millipore). Incubation of primary and secondary antibodies was carried out at 4  $^{\circ}$ C overnight. Protein labeling was visualized by enhanced chemiluminescence.

**Plasma Membrane Surface Biotinylation.** Biotinylation of plasma membrane proteins was achieved in fresh 1 mg/ml solution of EZ-Link Sulfo-NHS-SS-Biotin (#89881; Pierce, Thermo Fisher Scientific). Homogenization of cell lysates in 1 ml lysis buffer (50 mM Tris, pH 7.5, 5 mM EDTA, 15 mM NaCl, 1% Triton, 1  $\times$  Protease inhibitor cocktail) (#04693116001; Roche) was done by passing the lysate through a 27 and subsequently a 30-gauge needle. After incubation with streptavidin beads (Thermo Fisher Scientific), biotinylated proteins were eluted and subjected to SDS/PAGE.

**Immunofluorescence Labeling.** Sperm suspension (air-dried on a microscope slides) or hiPSC-RPE cells (grown on transwell-filters for 2–3 mo) were fixed in 4% (wt/vol) paraformaldehyde/PBS for 10 min and blocked by PBS containing 0.3% Triton X-100 and 10% (vol/vol) goat serum. Incubation with primary antibody was performed overnight followed by labelling with fluorescent-conjugated secondary antibody for 2 h at room temperature. Stained spermatozoa or hiPSC-RPE cells were imaged on a Zeiss confocal microscope LSM 510 (Zeiss).

**Sperm Phenotype.** Sperm preparation, evaluation of sperm viability and acrosome integrity, sperm tail morphology and motility including a quantitative analysis are described in detail in *SI Materials and Methods*.

**Xenopus Laevis Oocyte Analysis.** Human (NM\_004183.3) and mouse (NM\_011913.2) BEST1 cDNAs were cloned into the *X. laevis* oocyte expression vector pTLN. Capped RNA was synthesized by in vitro transcription with Sp6 RNA polymerase. Oocytes from *X. laevis* were prepared as described (33) and were thoroughly defolliculated and monitored for endogenous swelling-activity. Membrane currents were measured by voltage clamping (oocyte clamp amplifier; Warner Instruments LLC) in intervals from –80 to +60 mV, in steps of 20 mV, each 1 s (*SI Materials and Methods*).

**Generation of hiPSC Cells and Differentiation to RPE.** A detailed procedure has been described previously (38).

**Patch-Clamp Recordings of Whole-Cell Currents.** hiPSC-RPE cells were trypsinized and seeded on poly-L-lysine coated glass cover slips. A detailed procedure for patch-clamp recordings is given in *SI Materials and Methods*.

**Short Hairpin RNA-Mediated Stable Gene Knockdown.** LRRc8A shRNA were inserted into the pLKO.1 vector (Addgene) (oligonucleotides: forward 5'-CCG GAC CAA GCT CAT CGT CCT CAA CCT CGA GGT TGA GGA CGA TGA GCT TGG TTT TTT G-3' and reverse 5'-AAT TCA AAA AAC CAA GCT CAT CGT CCT CAA CCT CGA GGT TGA GGA CGA TGA GCT TGG T-3'). A detailed procedure is given in *SI Materials and Methods*.

**Statistical Analysis.** Statistical analysis was performed applying the Wilcoxon signed rank test for nonnormal distribution and Student's *t* test for normal distribution by IGOR PRO software (WaveMetrics). For box plots, the whiskers reach the 5th and 95th percentiles of the range.  $P < 0.05$  was considered statistically significant.

kers reach the 5th and 95th percentiles of the range.  $P < 0.05$  was considered statistically significant.

**ACKNOWLEDGMENTS.** We thank Timo Strünker, Luis Alvarez, and Christoph Brenker (Department of Molecular Sensory Systems) for help with sperm motility experiments and for critically reading the manuscript; M. Landthaler (Department of Dermatology, University Hospital Regensburg) and L. Bruckner-Tuderman and J. S. Kern (Department of Dermatology, University Hospital Freiburg) for providing human skin biopsies; M. Breunig and A. Göpferich (Department of Pharmaceutical Technology, University of Regensburg) for help with confocal microscopy; T. Jahner for technical assistance; and E. Röhl for help with ocular phenotyping of Best<sup>-/-</sup> mice. This work was supported in part by Grant 3625340 from Novartis Pharma, Germany (to C.B. and B.H.F.W.), German Research Foundation (DFG) Grants WE1259/20-1 (to B.H.F.W.) and WE2298/4-1 (to C.H.W.), DFG SFB699 Projects A7 and A12 (to K.K.), and Volkswagenstiftung 87499 (to K.K.).

- Lang F, et al. (1998) Functional significance of cell volume regulatory mechanisms. *Physiol Rev* 78(1):247–306.
- Nilius B, et al. (1997) Properties of volume-regulated anion channels in mammalian cells. *Prog Biophys Mol Biol* 68(1):69–119.
- Chien LT, Zhang ZR, Hartzell HC (2006) Single Cl<sup>-</sup> channels activated by Ca<sup>2+</sup> in Drosophila S2 cells are mediated by bestrophins. *J Gen Physiol* 128(3):247–259.
- Fischmeister R, Hartzell HC (2005) Volume sensitivity of the bestrophin family of chloride channels. *J Physiol* 562(Pt 2):477–491.
- Kunzelmann K, et al. (2011) Role of the Ca<sup>2+</sup>-activated Cl<sup>-</sup> channels bestrophin and anoctamin in epithelial cells. *Biol Chem* 392(1-2):125–134.
- Qiu Z, et al. (2014) SWELL1, a plasma membrane protein, is an essential component of volume-regulated anion channel. *Cell* 157(2):447–458.
- Voss FK, et al. (2014) Identification of LRRc8 heteromers as an essential component of the volume-regulated anion channel VRAC. *Science* 344(6184):634–638.
- Stöhr H, Marquardt A, Nanda I, Schmid M, Weber BH (2002) Three novel human VMD2-like genes are members of the evolutionary highly conserved RFP-TM family. *Eur J Hum Genet* 10(4):281–284.
- Marquardt A, et al. (1998) Mutations in a novel gene, VMD2, encoding a protein of unknown properties cause juvenile-onset vitelliform macular dystrophy (Best's disease). *Hum Mol Genet* 7(9):1517–1525.
- Petrukhin K, et al. (1998) Identification of the gene responsible for Best macular dystrophy. *Nat Genet* 19(3):241–247.
- Mohler CW, Fine SL (1981) Long-term evaluation of patients with Best's vitelliform dystrophy. *Ophthalmology* 88(7):688–692.
- Cross HE, Bard L (1974) Electro-oculography in Best's macular dystrophy. *Am J Ophthalmol* 77(1):46–50.
- Hartzell HC, Qu Z, Yu K, Xiao Q, Chien LT (2008) Molecular physiology of bestrophins: Multifunctional membrane proteins linked to best disease and other retinopathies. *Physiol Rev* 88(2):639–672.
- Sun H, Tsunenari T, Yau KW, Nathans J (2002) The vitelliform macular dystrophy protein defines a new family of chloride channels. *Proc Natl Acad Sci USA* 99(6):4008–4013.
- Neusser R, Muller C, Milenkovic VM, Strauss O (2010) The presence of bestrophin-1 modulates the Ca<sup>2+</sup> recruitment from Ca<sup>2+</sup> stores in the ER. *Pflugers Archiv* 460(1):163–175.
- Marmorstein LY, et al. (2006) The light peak of the electroretinogram is dependent on voltage-gated calcium channels and antagonized by bestrophin (best-1). *J Gen Physiol* 127(5):577–589.
- Lee S, et al. (2010) Channel-mediated tonic GABA release from glia. *Science* 330(6005):790–796.
- Woo DH, et al. (2012) TREK-1 and Best1 channels mediate fast and slow glutamate release in astrocytes upon GPCR activation. *Cell* 151(1):25–40.
- Krämer F, Stöhr H, Weber BH (2004) Cloning and characterization of the murine Vmd2 RFP-TM gene family. *Cytogenet Genome Res* 105(1):107–114.
- Singh R, et al. (2013) iPSC cell modeling of Best disease: Insights into the pathophysiology of an inherited macular degeneration. *Hum Mol Genet* 22(3):593–607.
- Stotz SC, Clapham DE (2012) Anion-sensitive fluorophore identifies the Drosophila swell-activated chloride channel in a genome-wide RNA interference screen. *PLoS ONE* 7(10):e46865.
- Chien LT, Hartzell HC (2008) Rescue of volume-regulated anion current by bestrophin mutants with altered charge selectivity. *J Gen Physiol* 132(5):537–546.
- Ren D, et al. (2001) A sperm ion channel required for sperm motility and male fertility. *Nature* 413(6856):603–609.
- Xu WMM, et al. (2007) Cystic fibrosis transmembrane conductance regulator is vital to sperm fertilizing capacity and male fertility. *Proc Natl Acad Sci USA* 104(23):9816–9821.
- Darszon A, et al. (2006) Sperm channel diversity and functional multiplicity. *Reproduction* 131(6):977–988.
- Cocquet J, et al. (2010) Deficiency in the multicopy Sycp3-like X-linked genes Slx and Slx1 causes major defects in spermatid differentiation. *Mol Biol Cell* 21(20):3497–3505.
- O'Shaughnessy PJ, Fleming L, Baker PJ, Jackson G, Johnston H (2003) Identification of developmentally regulated genes in the somatic cells of the mouse testis using serial analysis of gene expression. *Biol Reprod* 69(3):797–808.
- Yeung CH, Sonnenberg-Riethmacher E, Cooper TG (1998) Receptor tyrosine kinase c-ros knockout mice as a model for the study of epididymal regulation of sperm function. *J Reprod Fertil Suppl* 53:137–147.
- Yeung CH, Sonnenberg-Riethmacher E, Cooper TG (1999) Infertile spermatozoa of c-ros tyrosine kinase receptor knockout mice show flagellar angulation and maturational defects in cell volume regulatory mechanisms. *Biol Reprod* 61(4):1062–1069.
- Joseph A, Shur BD, Ko C, Chambon P, Hess RA (2010) Epididymal hypo-osmolality induces abnormal sperm morphology and function in the estrogen receptor alpha knockout mouse. *Biol Reprod* 82(5):958–967.
- Yeung CH, et al. (2002) Sperm volume regulation: Maturation changes in fertile and infertile transgenic mice and association with kinematics and tail angulation. *Biol Reprod* 67(1):269–275.
- Navarro B, Miki K, Clapham DE (2011) ATP-activated P2X2 current in mouse spermatozoa. *Proc Natl Acad Sci USA* 108(34):14342–14347.
- Ackerman MJ, Wickman KD, Clapham DE (1994) Hypotonicity activates a native chloride current in Xenopus oocytes. *J Gen Physiol* 103(2):153–179.
- Morin XK, Bond TD, Loo TW, Clarke DM, Bear CE (1995) Failure of P-glycoprotein (MDR1) expressed in Xenopus oocytes to produce swelling-activated chloride channel activity. *J Physiol* 486(Pt 3):707–714.
- De La Fuente R, Namkung W, Mills A, Verkman AS (2008) Small-molecule screen identifies inhibitors of a human intestinal calcium-activated chloride channel. *Mol Pharmacol* 73(3):758–768.
- Martins JR, et al. (2011) Anoctamin 6 is an essential component of the outwardly rectifying chloride channel. *Proc Natl Acad Sci USA* 108(44):18168–18172.
- Johnson AA, et al. (2013) Differential effects of Best disease causing missense mutations on bestrophin-1 trafficking. *Hum Mol Genet* 22(23):4688–4697.
- Brandl C, et al. (2014) In-depth characterisation of Retinal Pigment Epithelium (RPE) cells derived from human induced pluripotent stem cells (hiPSC). *Neuromolecular Med* 16(3):551–564.
- Anderson JW, Jirsch JD, Fedida D (1995) Cation regulation of anion current activated by cell swelling in two types of human epithelial cancer cells. *J Physiol* 483(Pt 3):549–557.
- Kunzelmann K, Milenkovic VM, Spitzner M, Soria RB, Schreiber R (2007) Calcium-dependent chloride conductance in epithelia: Is there a contribution by Bestrophin? *Pflugers Archiv* 454(6):879–889.
- Milenkovic VM, Röhl E, Weber BH, Strauss O (2011) Disease-associated missense mutations in bestrophin-1 affect cellular trafficking and anion conductance. *J Cell Sci* 124(Pt 17):2988–2996.
- Kirichok Y, Lishko PV (2011) Rediscovering sperm ion channels with the patch-clamp technique. *Mol Hum Reprod* 17(8):478–499.
- Zeng XH, Yang C, Kim ST, Lingle CJ, Xia XM (2011) Deletion of the Slo3 gene abolishes alkalization-activated K<sup>+</sup> current in mouse spermatozoa. *Proc Natl Acad Sci USA* 108(14):5879–5884.
- Voets T, Droogmans G, Raskin G, Eggemont J, Nilius B (1999) Reduced intracellular ionic strength as the initial trigger for activation of endothelial volume-regulated anion channels. *Proc Natl Acad Sci USA* 96(9):5298–5303.
- Cooper TG (2011) The epididymis, cytoplasmic droplets and male fertility. *Asian J Androl* 13(1):130–138.